Niklas Bauer[1,*]
Matthias Baumann[2]
Simon Feldmeth[2]
Frank Bauer[2]
Katharina Schmitz[1]

Elastohydrodynamic Simulation of Pneumatic Sealing Friction Considering 3D Surface Topography

This contribution presents an elastohydrodynamic lubrication (EHL) model for pneumatic spool valves. For an accurate estimation of the transient friction of this tribological sealing system, the surface topography of the cylindrical sealing counterfaces of the valve housings are measured and analyzed with an optical surface measurement instrument. Based on the surface topography data, tribological properties and flow factors of the system are derived. It has been found that the consideration of the surface topography has a significant influence on the simulation results of the EHL model, lowering the calculated friction force by up to 20 %.

Keywords: Elastohydrodynamic lubrication, Pneumatic sealing friction, Pneumatic spool valves, Surface topography, Tribological sealing system

Received: October 03, 2022; *accepted:* November 10, 2022

DOI: 10.1002/ceat.202200471

Supporting Information available online

1 Introduction

1.1 Motivation

The frictional behavior of seals determines the functional behavior in many applications. Translational pneumatic seals are widely used in pneumatic switching elements. However, the precise functional relationships between the frictional behavior and the characteristic properties of the components and materials used are still unknown. The frictional behavior varies with the many different operating conditions found in practice, so that large series of experiments would have to be conducted to accurately describe the dynamic of the seal. However, empirical investigations are time-consuming and expensive. For this reason, an elastohydrodynamic lubrication (EHL) simulation model was modified for the calculation of translational pneumatic seals and extended to include the corresponding material and component characteristics.

The aim of the procedure is to calculate and predict the friction of the valve. These results can be used to improve the system behavior of pneumatic elements and to compensate for changes in the system based on the current system state. In the presented investigation, the influence of the anisotropic surface structure implemented by the flow factors as proposed by Patir and Cheng [1, 2] shall be determined. In [3], it has been shown for hydraulic sealing contacts that the flow factors can have a negligible or a rather important influence on the calculated friction force depending on the operating conditions and the contact partners. Therefore, in this contribution it is investigated if the consideration of flow factors has a significant influence on the simulation result for a sealing contact within a pneumatic spool valve. Based on this study, it can be decided whether the anisotropy of the surface roughness has to be considered for a simulation model of the investigated sealing contact or whether a simplified characterization of the contact partners without the calculation of flow factors provides results of comparable accuracy.

1.2 Pneumatic Valves

Fig. 1 shows a sectional view of a pneumatic spool valve. It consists of a spool within a housing with several ports. In pneumatic systems, these valves are used to control the air flow between components.

During operation, the spool moves within the housing actuated either with a solenoid or pneumatically by the pilot valve. The position of the spool determines which ports are connected to or disconnected from each other. To prevent internal and external leakage, two different kinds of seals are placed on the spool. The inner seals (1) make or lose contact to the housing depending on the position of the spool and are employed in the switching operations to open or close the respective air ports. The two outer seals (2) are always in contact with their

[1]Niklas Bauer https://orcid.org/0000-0002-5520-0611,
Prof. Dr.-Ing. Katharina Schmitz
https://orcid.org/0000-0002-1454-8267
(niklas.bauer@ifas.rwth-aachen.de)
RWTH Aachen University, Institute for Fluid Power Drives and Systems (ifas), Campus-Boulevard 30, 52074 Aachen, Germany.
[2]Dr.-Ing. Matthias Baumann https://orcid.org/0000-0002-1962-5153,
Simon Feldmeth https://orcid.org/0000-0003-0018-0710,
Prof. Dr.-Ing. Frank Bauer https://orcid.org/0000-0001-7799-7628
University of Stuttgart, Institute of Machine Components (IMA), Pfaffenwaldring 9, 70569 Stuttgart, Germany.

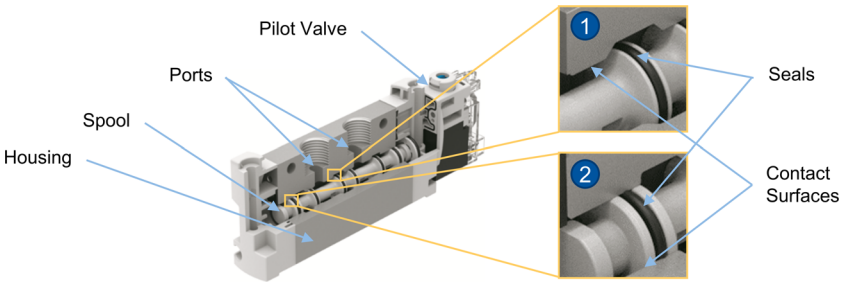

Figure 1. Pneumatic spool valve. Picture provided by courtesy of Festo [4].

counter surfaces and seal the pressurized air against the environment. During operation, the relative movement of the seals on their respective counter surfaces causes friction. The aim of the presented research is the calculation of the friction within the contact between the housing and the inner seals (1).

2 Materials and Methods

2.1 Research Approach

To describe the transient seal friction in the valve system, an EHL simulation model is used. To achieve a modeling of the system that is as realistic as possible, the system components are comprehensively characterized with regard to their properties before modeling. This specifically includes the measurement of the surface characteristics of the contacting cylindrical valve housing surfaces.

2.2 Specimen and Preparation

The project partner company provided six identical valve housings, which were specifically manufactured for the investigations to be carried out within this analysis. Each housing has a total of six cylindrical sealing seats inside the housing bore, on which the connections between the corresponding ports are switched. To reach the cylindrical surfaces by means of an optical surface measuring instrument, three of the housings were cut open in longitudinal horizontal section and the other three in longitudinal vertical section, using a diamond wire saw. This way, 6×6×2 = 72 cylindrical surfaces were created to be characterized metrologically (see Fig. 2).

Each cylindrical surface is measured on two halves of the housing each. This allows the potential scattering of the surface properties to be considered. The two corresponding cylindrical surfaces are referred to according to the type of the separation cut with the designations “c” and “d” or “e” and “f” as well as with a surface number from 1 to 6. The two outer surfaces 1 and 6 are in steady contact with the outer seals marked with (2) in Fig. 1. The surfaces 2 to 5 form the counter faces for the inner seals marked with (1) in Fig. 1 and are thus in the focus of this analysis.

2.3 Surface Measurement – Methods and Equipment

To measure the cylinder surfaces, a white light interferometer (WLI) type NPFLEX-LA from Bruker was used. All six cylinder surfaces of each valve housing were measured in the cylinder base with a rectangular measuring area, stitched together from several individual measurements. A 10× Linnik interferometer objective was used, whose working distance enables the measurement of the samples without further sample preparation. The measurement resolution is 0.64 µm in lateral direction. An exemplary illustration of a cylinder housing with assigned representations of surface topographies is displayed in the Supporting Information (Fig. S1).

For the evaluation of the measurement data and the computation of surface parameters, the software Mountains Map from Digital Surf was used. The evaluation procedure is shown afterwards in Fig. 3. For the comparative analysis of the surface properties, an evaluation area of 0.3–1.8 mm was defined, which is first cut out from the respective raw data. A second-order polynomial fit to the surface topography is applied to filter the cylindrical shape of the measurement data. Since WLI measurement data tends to exhibit measurement artifacts, such as spikes and batwings, the evaluation considers a core area of the surface material ratio of 0.5–99.5 % of the areal material ratio curve. This is achieved via a threshold filter.

Non-measured data points are filled via a spline interpolation. A further median filter reduces high-frequency measurement artifacts. Based on this evaluation procedure, three-dimensional surface parameters are derived. Additional two-dimensional parameters are derived from further extracted profile traces in axially direction. To match a standardized filter cut-off wavelength of 0.25 mm, the profile traces are limited to an evaluation length of 1.25 mm.

2.4 Simulation Model

For modeling the pneumatic seal in the spool valve, the simulation model ifas-DDS [3] is used. The monolithic simulation

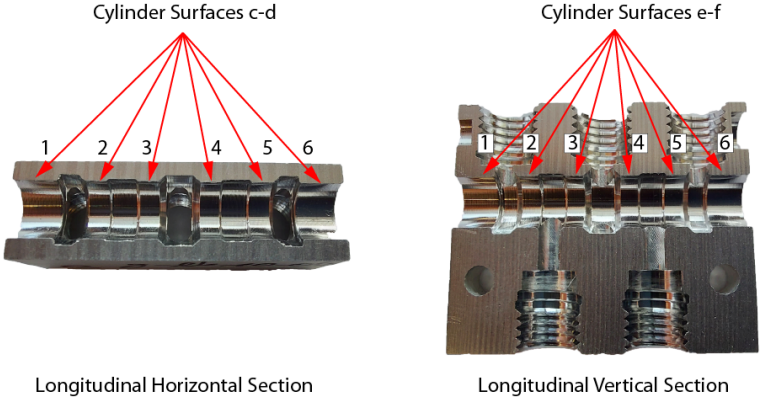

Figure 2. Preparation of cylinder valve housings for optical measurement.

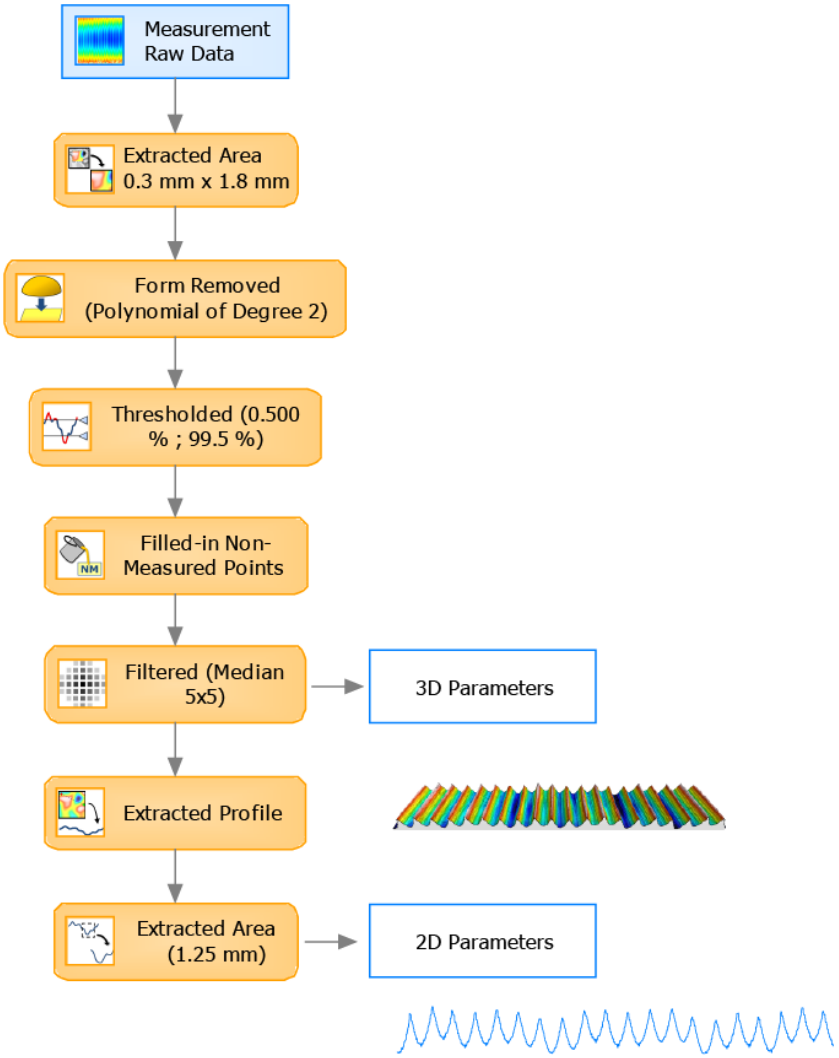

Figure 3. Evaluation scheme of the optical topographic measurement data.

model is based on the commercial FEM-software Abaqus [5] extended by user subroutines to implement the hydrodynamic pressure buildup and custom solid contact behavior. The fluid pressure within the sealing contact is modeled using the Reynolds equation solved by a finite difference scheme. In the past, the model has been used to calculate the friction force of reciprocating hydraulic seals [6] and macroscopic wear geometries [7]. The ifas-DDS contains the Jakobsson-Floberg-Olsson cavitation model [8, 9] using the implementation according to Woloszynski [10] to model the influence of cavitation. Further details of the implementation are given in [11].

2.5 Implementation of Surface Roughness

The surface roughness is considered by the simulation model in two different ways. First, the roughness has an effect on the solid contact mechanics, which describe the normal and tangential force at each node in contact. These forces can be calculated if the functions of solid contact pressure p_c[1)] and the real area of contact A_{real} are known for each separation h. Second, the roughness also affects the lubrication and the fluid pressure within the contact since the structure of the surface roughness influences the lubricant flow. This can be taken into account by the flow factor model as described by Patir and Cheng [1, 2].

For an axisymmetric case, this approach introduces two flow factors into the Reynolds equation. The first one is the pressure flow factor Φ_p, which characterizes how the pressure flow is affected by the surface structure by scaling the Poiseuille flow term of the Reynolds equation. For surface structures oriented in the direction of the pressure gradient this factor is higher than for structures oriented perpendicular to the pressure flow. In contrast, the shear flow factor Φ_s considers the transport of fluid due to the movement of the roughness by increasing the Couette term of the Reynolds equation. The complete Reynolds equation used for this contribution is given in Eq. (1):

$$\frac{v_{rel}}{2}\frac{\partial}{\partial x}[(1-\theta)\rho h + (1-\theta)\rho R_a \Phi_s] - \frac{\partial}{\partial x}\left[\frac{(1-\theta)\rho h^3}{12\eta}\Phi_p \frac{\partial p}{\partial x}\right] + \frac{\partial}{\partial t}[(1-\theta)\rho h] = 0 \quad (1)$$

The influence on the pressure buildup for an anisotropic surface with grooves is illustrated in Fig. 4. If the grooves on the surface are oriented circumferentially, i.e., perpendicularly to the relative movement, the pressure flow is reduced by the surface topography. Therefore, a higher hydrodynamic pressure can be built up in the sealing contact since the grooves effectively act as a pressure barrier to the outside.

In addition, the shear flow is supported by the perpendicular grooves due to the additional amount of lubricant which is transported within the grooves. Due to the increased supply with lubricant, the additional shear flow also supports the pressure buildup in the sealing contact. For surfaces with axial grooves, i.e., parallel to the movement, the opposite is true: the structures support the pressure flow and reduce the shear flow, both of which effects lower the hydrodynamic pressure in the contact.

For calculating the flow factors, the module MicroSim of the software Tribo-X has been used [12]. The module calculates the flow factors with multiple EHL simulations, each for a

1) List of symbols at the end of the paper.

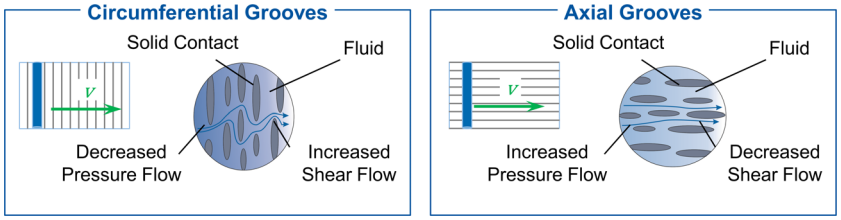

Figure 4. Illustration of the influence of the flow factors.

different separation of the surfaces. For that, deformation and pressure distribution due to an exemplary pressure gradient or relative movement are calculated for the rough surfaces. Afterwards, the resulting shear or pressure flow are calculated and compared to the flow between two ideally rough surfaces. The flow factors are then chosen so that their respective correction terms adjust the shear and pressure flow between the smooth surfaces so that they are the same as between the rough surfaces. Further details on the calculation approach are described in [13].

For the calculation of the contact mechanics and the flow factors, the rubber surface was assumed to be ideally smooth. As for the material values, Young's moduli of $E_{\mathrm{Steel}} = 210\,000$ MPa and $E_{\mathrm{Rubber}} = 12.5$ MPa and Poisson's ratios of $\nu_{\mathrm{Steel}} = 0.3$ and $\nu_{\mathrm{Rubber}} = 0.5$ were chosen for the steel and the rubber, respectively. As input data for the simulation, sample areas of the measured surfaces with 300×300 points were chosen.

2.6 Simulation Setup

The presented mesh, boundary conditions, and material properties have been used in an earlier publication [14] to determine the influence of different non-Newtonian viscosity models. The following description of these parameters has been taken from the aforementioned publication.

The sealing system was modeled as axisymmetric. Geometry and mesh of the simulation model are depicted in Fig. 5. The model consists of the three parts seal, housing, and spool. The inner and outer radius of the seal in assembled condition are about 1.4 and 3 mm with a length of about 0.72 mm in axial direction. The geometry of the spool has been adjusted so that there is no axial clearance between the seal and the spool to prevent axial movement between the seal and the spool after assembly. The chamfers on the housing were neglected. Instead, the housing was modeled as a cylindrical surface with constant diameter so that the seal is always in contact to its counterface. The seal is meshed with 6066 nodes and 5800 first-order axisymmetric hybrid elements.

The number of elements for which the Reynolds equation is solved is 200. The housing and the spool are modeled as analytical rigid surfaces. As mentioned earlier, the different diameters within the housing are neglected, so that it can be represented by a cylindrical surface. The seal is modeled as an incompressible hyperelastic Mooney-Rivlin material with $C_{10} = 0$ MPa and $C_{01} = 1.78$ MPa. Outside the seal, atmospheric pressure was assumed. Cavitation was assumed to occur at a relative pressure of –0.1 MPa.

For the contact between spool and seal the exponential contact behavior in Abaqus was employed. To restrict relative movement between the two parts, a constant coefficient of friction of $\mu = 0.2$ was applied. The normal contact pressure between seal and housing is given by the averaged contact pressure curve. The tangential stresses were calculated based on the averaged real area of contact assuming a shear stress of $\tau_{\mathrm{cont}} = 1.5$ MPa acting on the real area of contact. Both contact pressure curve and real area of contact between seal and housing are presented in Sect. 3.2. For the fluid, a dynamic viscosity of 87.2 mPa s was chosen. This corresponds to a Newtonian approximation of the shear viscosity of the grease at 50 °C for the chosen operating condition [14]. The pressure and shear flow factors used are given in Sect. 3.2. To compare the influence of each flow factor individually, the simulation has been performed once without flow factors as a reference, once for each of the two flow factors, and a fourth time using both flow factors.

As for initial and boundary conditions, spool and housing are placed in radial distance from the seal so that no contact occurs. During the first step of the simulation, the system is assembled by moving the analytical rigids into their final positions thereby prestressing the sealing contact, see Fig. 5 (right). In the next step, the spool faces are accelerated with a constant acceleration up to a velocity of 700 mm s^{-1} within 1.5 ms. Immediately after reaching the maximum velocity, the acceleration is inverted until the seal reaches a velocity of –700 mm s^{-1} in the opposite direction. This process is repeated multiple times so that the friction force reaches a steady-state oscillation.

During the first acceleration and deceleration period, much higher friction forces happen than during the rest of the simulation. This is because the lubricant film needs some time to build up. Before that, a high amount of solid friction occurs as due to the assembly in the simulation, no lubricant is present in the contact at the start of the simulation. It is expected that this effect is a lot less severe in reality, since the contact is never completely dry even after long standstill periods. For that reason, the friction is not evaluated during the first acceleration and deceleration period. After that period, the friction forces were the same for all following periods.

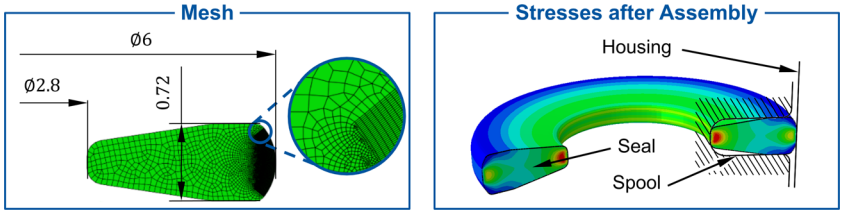

Figure 5. Left: Mesh of the seal and measurements (mm) of the assembled seal. Right: Stresses after assembly of spool and housing. Spool and housing are shown as lines on the right part of the figure.

3 Results

The results of the surface measurements and simulations are described below. All subsequent representations of surface parameters are shown normalized to the mean value of the specific range of values.

3.1 Surface Topography Measurement

Fig. 6 illustrates one exemplary three-dimensional surface topography of a valve housing, prepared according to the procedure displayed in Sect. 2.3, in detail. The surfaces are manufactured with a turning process, which can be seen clearly by the axially periodic surface structure. The pneumatic seal is therefore moved in operation mainly in an orthogonal direction to the structure orientation. In addition to the roughness and waviness of the surface, the periodicity of the rotational structure must therefore be explicitly considered for further studies.

The structure periodicity of all measured surfaces, which can be evaluated, e.g, with the roughness parameter *Rsm* shown in Fig. 7a, are extremely well reproducible. The relative deviations of the individual values to the group mean range from –2 to 4 %. The manufacturing process is thus optimally controlled with regard to axial feed. In terms of surface roughness, shown by the *Rz* values in Fig. 7b, there are some fluctuations with normalized values of *Rz* between 0.85 and 1.14 (corresponding to a relative deviation of approx. ±15 %). This can, however, be regarded as normal, since *Rz* values generally tend to have a higher scatter as stronger averaging parameters such like *Ra*. The *Ra* values, illustrated in Fig. 8, show a slight difference in the surface roughness of the surfaces 1–3 to the surfaces 4–6, what can be seen particularly well by the normalized representation at this point. Nevertheless, the surface roughness of all measured surfaces can be regarded as highly comparable so far.

An advantage of 3D surface parameters can be seen when looking at the normalized *Sz* values of the measured surfaces, shown in Fig. 8. The specifications of the 3D parameters (DIN EN ISO 25178) allow a wide scope for the evaluation of measurement data. There are no exact regulations regarding the filtering. This is to be developed rather application-dependently. The *Sz* value displayed here is calculated as the height difference of the measured values considered over the entire evaluation area of 0.3×1.8 mm. No filtering into roughness and waviness is carried out, which means that the parameter corresponds more to the *Pt* value in the classic roughness evaluation,

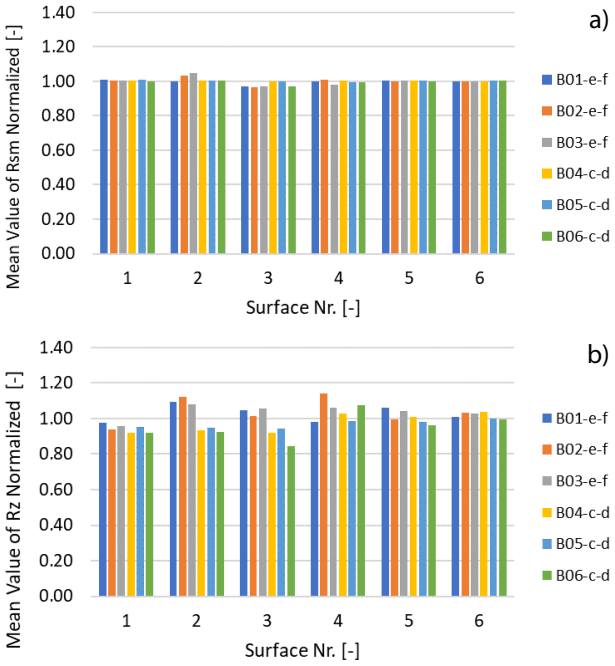

Figure 7. Normalized mean values of *Rsm* (left) and *Rz* (right) of two measured housing halves for each cylinder surface, measurement data obtained by optical surface measurement (WLI).

but with the difference that significantly more measured values are included via an areal analysis, and the values are therefore statistically better founded.

The *Sz* values thus represent the primary surface and show that the surfaces though very reproducible in terms of roughness, exhibit some differences with regard to long-wave, higher amplitude structure components. The normalized *Sz* parameter shows values between 0.81 and 1.32, which is a relative deviation from –19 to 32 %. The range is above the previously shown *Rz* values and indicates that some of the surfaces exhibit waviness structures. This can be seen quite clearly in the surfaces presented in Fig. 6. If roughness parameters were considered exclusively, as is often the case, this existing spread would not be evident. An additional consideration of waviness or primary profile characteristics would be necessary. Three-dimensional measurement data enables the evaluation of all surface properties at once. The data is thus provided and evaluated as required.

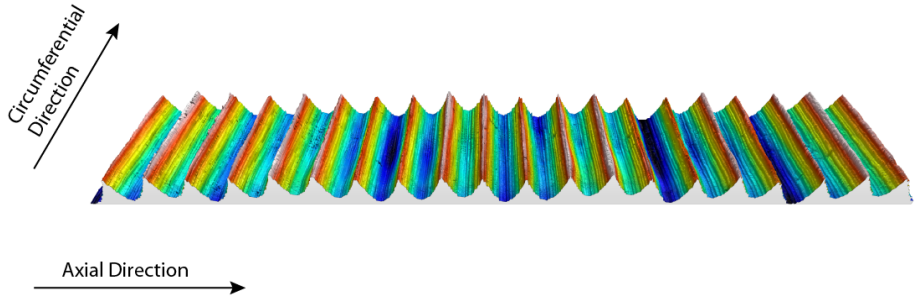

Figure 6. Three-dimensional surface topography of one exemplary cylinder surface.

3.2 Calculated Model Parameters

It has been demonstrated that all measured surfaces in general show similar characteristics concerning the surface roughness and the frequency of the periodical surface structure. For that reason, a single valve housing has been chosen for further investigation. Based on the

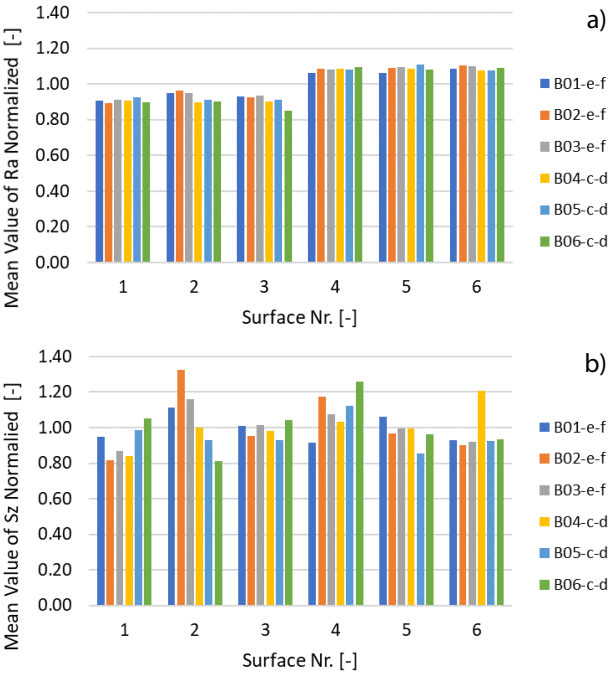

Figure 8. Normalized mean values of *Ra* (a) and *Sz* (b) of two measured housing halves for each cylinder surface, measurement data obtained by optical surface measurement (WLI).

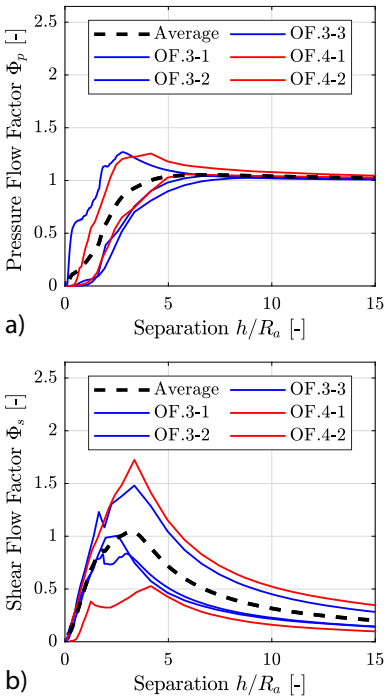

Figure 9. Calculated values and averages for pressure (a) and shear flow factor (b).

given range of *Sz* values of the measured specimen as shown in Fig. 8, specimen B03 has been selected as representative, since its values are close to the average of all measurements. Since only small 300×300 sample areas are used for the calculation of the simulation input, five different positions have been chosen on two surfaces of the valve to average the surface characteristics.

In the following figures, these samples are referenced by the number of the surface as defined in Fig. 2 followed by the number of the sample on the surface (e.g., Surf.3-1 was calculated based on the first sample of surface 3). For averaging, the arithmetic mean value of all measurements was calculated for each separation. If no data was given for a certain separation, cubic interpolation was used. The curves of nominal contact pressure p_c and the fraction of the real area of contact A_{real} as functions of the separation h are shown in Fig. S2.

The results for the pressure flow factor Φ_p and the shear flow factor Φ_s and their respective average curves are presented in Fig. 9. For all figures within this paper, the separation is defined as the distance between the mean lines of the deformed contact surfaces. Since the pressure flow factor is smaller than 1 for most separations, the pressure flow is in general expected to be hampered by the asperities. This is in line with the expectations as due to the manufacturing process the surface has a clearly visible structure perpendicular to the direction of the pressure gradient.

3.3 Simulation Results

Fig. 10a shows the total friction force (solid lines) and its components, the fluid (dotted) and solid friction force (dash-dotted line), for the simulation without flow factors and with both flow factors. For a better comparison, all friction forces in this contribution have been normalized by division with the maximum of the friction force F_0 without flow factors. The solid friction is considerably higher than the fluid friction and shows a hysteresis around the center which is also visible for the total friction force. Comparing the simulations with and without flow factors it can be seen that the inclusion of flow factors reduces both components of the friction force. Overall, the maximum of the total friction force gets reduced by up to 20 %.

Fig. 10b shows the separation in the sealing contact at the maximum relative velocity v_{rel} = 700 mm s^{-1}. The largest separation is predicted with the simulation including both pressure and shear flow factor. When considering each flow factor individually, both pressure and shear flow factor lead to roughly similar separations in the sealing contact at the maximum velocity.

To investigate the effects of each flow factor individually, two additional simulations were executed: one of them using only the pressure flow factor Φ_p, the other simulation using only the shear flow factor Φ_τ. The calculated friction forces are indicated in the Supporting Information. A comparison yields that the inclusion of either flow factor reduces the total friction force. The reduction at v_{rel} = 700 mm s^{-1} is nearly the same for both flow factors. However, for lower velocities, the reduction of the friction force in the simulation with the shear flow factor is considerably lower. The increasing effect of the shear flow factor for higher velocities can be explained by Eq. (1) since the term introducing the shear flow factor is proportional to the relative velocity.

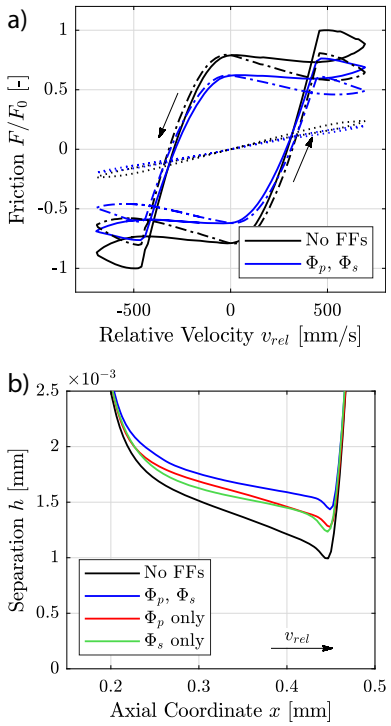

Figure 10. (a) Calculated total friction (solid lines), solid friction (dash-dotted lines), and fluid friction (dotted lines). (b) Separations h at v_{rel} = 700 mm s^{-1} for different flow factors.

4 Summary and Conclusion

This contribution presents an EHL simulation of the friction of the sealing contact within a pneumatic spool valve considering the surface topography of the counter surface. First, the surface topography was obtained through optical measurement. Using the measurement data, the tribological properties of the system such as normal contact pressure, real area of contact, and flow factors were calculated. Based on these properties, an EHL simulation of the contact was performed to quantify the influence of the surface topography represented by the flow factors.

It has been found that the usage of both, the pressure and the shear flow factor, leads to a significant decrease in friction force by up to 20 % which can be attributed to an improved hydrodynamic pressure buildup within the contact and thus a larger average separation. Therefore, it can be concluded that the surface topography has to be considered for an EHL simulation of the investigated sealing contact of a pneumatic spool valve in order to obtain accurate results of the friction force.

As a next step, it is planned to calculate the contact properties also for other measured surfaces and to compare the results obtained by TriboX to the results obtained by the contact mechanics theory of Persson [15, 16]. In addition, a test rig is currently under construction which will be used to compare the simulated friction forces to experimental measurements of the tribological system.

Supporting Information

Supporting Information for this article can be found under DOI: https://doi.org/10.1002/ceat.202200471.

Acknowledgment

The authors thank the Fluid Power Research Fund of the VDMA for its financial support (grant: FKM No. 7049610). Open access funding enabled and organized by Projekt DEAL.

The authors have declared no conflict of interest.

Symbols used

A_{real}	[%]	real area of contact
C_{10}, C_{01}	[MPa]	Mooney-Rivlin parameters of the seal (for the FEM)
E_{Rubber}	[MPa]	Young's modulus of the seal (for calculation of the flow factors)
E_{Steel}	[MPa]	Young's modulus of the counter surface (for calculation of the flow factors)
F_0	[N]	maximum of the total friction force for the simulation without flow factors
h	[mm]	separation in the sealing contact
p	[MPa]	fluid pressure in the sealing contact
p_c	[MPa]	normal contact pressure
Pt	[µm]	total profile height of the primary surface profile
Ra	[µm]	arithmetic mean deviation of the roughness profile
R_q	[µm]	root mean squared roughness
Rsm	[mm]	mean width of the roughness elements
Rz	[µm]	average roughness depth
Sz	[µm]	maximum height difference
t	[s]	time
v_{rel}	[mm s^{-1}]	relative velocity in the sealing contact
x	[mm]	coordinate in axial direction

Greek letters

η	[Pa s]	viscosity of the lubricant
θ	[–]	cavity fraction
λ_C	[mm]	cut-off wavelength Gaussian roughness filter
μ	[–]	constant coefficient of friction between seal and spool
ν_{Rubber}	[–]	Poisson's ratio of the seal (for the calculation of the flow factors)
ν_{Steel}	[–]	Poisson's ratio of the counter surface (for the calculation of the flow factors)

ρ	[kg m^{-3}]	density of the lubricant
τ_{cont}	[MPa]	shear stress acting on the real area of contact
Φ_p	[–]	pressure flow factor
Φ_s	[–]	shear flow factor

Abbreviations

EHL	elastohydrodynamic lubrication
ifas-DDS	dynamic sealing simulation model at ifas
WLI	white light interferometer

References

[1] N. Patir, H. S. Cheng, *J. Lubr. Technol.* **1978**, *100 (1)*, 12–17. DOI: https://doi.org/10.1115/1.3453103

[2] N. Patir, H. S. Cheng, *J. Lubr. Technol.* **1979**, *101 (2)*, 220–229. DOI: https://doi.org/10.1115/1.3453329

[3] J. Angerhausen, Physikalisch motivierte, transiente Modellierung translatorischer Hydraulikdichtungen, *Dissertation*, RWTH Aachen University **2020**.

[4] www.festo.com/net/SupportPortal/Files/381028/PSIplus_VTUG_en_V05_M.pdf (Accessed on August 12, 2021)

[5] *Abaqus 2021 Documentation*, Dassault Systems, Vélizy-Villacoublay, France **2021**.

[6] J. Angerhausen, H. Murrenhoff, J. Dorogin, B. N. J. Persson, M. Scaraggi, *The 10th JFPS Int. Symp. on Fluid Power*, Fukuoka, October **2017**.

[7] J. Angerhausen, M. Woyciniuk, H. Murrenhoff, K. Schmitz, *Tribol. Int.* **2019**, *134*, 296–307. DOI: https://doi.org/10.1016/j.triboint.2019.01.048

[8] B. Jakobsson, L. Floberg, *Trans. Chalmers Univ. Technol.* **1957**, *190*, 1–116.

[9] K.-O. Olsson, *Trans. Chalmers Univ. Technol.* **1965**, *308*, 59.

[10] T. Woloszynski, P. Podsiadlo, G. W. Stachowiak, *Tribol. Lett.* **2015**, *58 (1)*, 839. DOI: https://doi.org/10.1007/s11249-015-0487-4

[11] N. Bauer, A. Rambaks, C. Müller, H. Murrenhoff, K. Schmitz, *Int. J. Fluid Power* **2021**, *22 (2)*, 199–232. DOI: https://doi.org/10.13052/ijfp1439-9776.2223

[12] www.tribo-technologies.com/de/tribo-x (Accessed on September 20, 2021)

[13] D. Bartel, *Simulation von Tribosystemen*, Vieweg+Teubner, Wiesbaden **2010**.

[14] N. Bauer, S. Hahn, S. Feldmeth, F. Bauer, K. Schmitz, *Tribol. Schmierungstech.* **2021**, *68 (6)*, 20–28. DOI: https://doi.org/10.24053/TuS-2021-0034

[15] B. Persson, *Surf. Sci. Rep.* **2006**, *61 (4)*, 201–227. DOI: https://doi.org/10.1016/j.surfrep.2006.04.001

[16] B. N. J. Persson, M. Scaraggi, *Eur. Phys. J. E: Soft Matter Biol. Phys.* **2011**, *34 (10)*, 113. DOI: https://doi.org/10.1140/epje/i2011-11113-9

